Visualizing the Formation and Collapse of DNA Toroids

Bram van den Broek,[†△*] Maarten C. Noom,[†△] Joost van Mameren,[†] Christopher Battle,[‡] Fred C. MacKintosh,[†] and Gijs J. L. Wuite[†*]

[†]Department of Physics and Astronomy and Laser Centre, VU University, Amsterdam, The Netherlands; and [‡]Institute for Theoretical Physics, University of Amsterdam, Amsterdam, The Netherlands

ABSTRACT In living organisms, DNA is generally confined into very small volumes. In most viruses, positively charged multivalent ions assist the condensation of DNA into tightly packed toroidal structures. Interestingly, such cations can also induce the spontaneous formation of DNA toroids in vitro. To resolve the condensation dynamics and stability of DNA toroids, we use a combination of optical tweezers and fluorescence imaging to visualize in real-time spermine-induced (de)condensation in single DNA molecules. By actively controlling the DNA extension, we are able to follow (de)condensation under tension with high temporal and spatial resolution. We show that both processes occur in a quantized manner, caused by individual DNA loops added onto or removed from a toroidal condensate that is much smaller than previously observed in similar experiments. Finally, we present an analytical model that qualitatively captures the experimentally observed features, including an apparent force plateau.

INTRODUCTION

In virtually all forms of life, the DNA that stores the genetic information has to be compacted tightly to fit into the cell or nucleus. Because of their high negative charge, DNA segments strongly repel each other. In nature this problem is generally solved by positively charged molecules that mediate interactions, resulting in an attractive potential between DNA tracts. In sperm cells for instance, DNA compaction is governed by tiny arginine-rich proteins called protamines. In these and many other cell types, strongly positively charged polyamines like spermine (4+) and spermidine (3+) are also involved in the compaction of DNA (1,2).

In vitro, polyamines can cause DNA to undergo a sharp condensation phase transition (3–6). In this process, DNA molecules aggregate into highly ordered structures, generally with toroidal or rod-like shapes, consisting of many (circumferentially wound) DNA strands (7–11). Toroidal DNA condensates have raised particular interest because of their striking similarity with the morphology of compacted DNA found in viruses and sperm cells.

A large number of studies using (cryo)electron microscopy have revealed that in solution toroidal DNA condensates consist of many circumferentially wound and hexagonally packed DNA helices (7,9–12). The (outer) diameter of such DNA toroids is typically 100 nm, nearly independent of DNA length, condensation conditions, and condensing agent (5,6,9,12–16). Recent developments in the field of single-molecule biophysics have made it possible to directly measure the forces and energies involved in the process of DNA condensation and decondensation. Single-molecule pulling experiments on condensed DNA have shown a dramatic influence of condensing agents on the elasticity of DNA (17–19).

In bulk experiments, globular or rodlike condensates are readily formed, and only by careful addition of condensing agent are toroids the dominant species (20,21). However, in single-molecule experiments the structure of DNA condensates is generally assumed to be toroidal. Furthermore, positively charged molecules also mediate adhesion between DNA and (negatively charged) surfaces, possibly affecting the observed condensing behavior. How the shape and size of DNA condensates are affected by DNA tension and the proximity of surfaces remains unclear (17,18,22–25). Moreover, despite previous efforts little is known about the dynamics of toroid formation under tension and the stability of such a condensate. In addition, an extensive, quantitative understanding of DNA toroid formation dynamics will be pertinent to the development and optimization of applications based on DNA-condensation, such as gene therapy (26–28). Exploiting recent advances in single-molecule technology (29,30) we aim to address these issues.

MATERIALS AND METHODS

Reagents

Lambda phage dsDNA (Roche Applied Science, Indianapolis, IN) was biotinylated at both ends, as described previously (31). Spermine (Sigma-Aldrich, St. Louis, MO) was dissolved into distilled deionized water (milliQ) to a stock concentration of 100 mM and stored at 4°C. Spermine stock

Submitted August 20, 2009, and accepted for publication December 21, 2009.

△Bram van den Broek and Maarten C. Noom contributed equally to this work.

*Correspondence: bramvdbroek@physics.leidenuniv.nl or gwuite@few.vu.nl

Bram van den Broek's present address is Physics of Life Processes, Leiden Institute of Physics, Leiden University, Niels Bohrweg 2, 2333 CA, Leiden, The Netherlands.

Joost van Mameren's present address is JPK Instruments AG, Bouchéstrasse 12, 12435 Berlin, Germany.

Christopher Battle's present address is Drittes Physikalisches Institut, Georg-August-Universität, 37077 Göttingen, Germany.

Editor: Taekjip Ha.

0006-3495/10/05/1902/9 $2.00

doi: 10.1016/j.bpj.2009.12.4334

solutions were used for up to 2 weeks. In all experiments spermine was diluted to a final concentration of 100 μM to 1 mM in TE buffer containing 10 mM Tris and 1 mM EDTA, pH 7.5.

Experimental setup

The experimental setup used has been reported earlier (32). For the experiments reported here two optical traps were used. One stationary trap was used for force detection, whereas the other trap could be steered through the sample with nanometer precision using acousto-optical deflectors. The motion of the bead during DNA stretching and relaxation was continuous with speeds varying from 15 to 750 nm/s. Interbead distances were calculated in real-time by video image analysis at 8 Hz. Raw force data were sampled at 8 kHz and pre-averaged to 128 Hz before analysis. The combined dual optical trap and fluorescence excitation and detection system has been described previously (29). High-sensitivity fluorescence imaging is obtained using a 473 nm laser excitation source and a Cascade 512B CCD camera interfaced with the WinView software package (both from Roper Scientific). To leave the elastic properties of DNA unaffected and prevent interference of the (positively charged) fluorescent YOYO-1 with the condensation process (33,34), the number of dye molecules per DNA was kept low enough to prevent detectable dye-induced lengthening of the DNA (35). DNA condensation and decondensation was imaged without fluorescent dye in the solution, in a buffer containing $\leq$1 mM spermine, with an exposure time of 0.4 s. The size of observed DNA condensates in the fluorescence images is limited by diffraction of the excitation light (473 nm) and is spread out over several pixels. Its position along the DNA can however be extracted with subpixel precision by fitting the spot with a 2-D Gaussian (36).

Fluorescence analysis

From the fluorescence images, a kymograph was constructed. This was done by: i), selecting a narrow box encompassing the DNA contour in all frames; ii), integrating the pixel values across the DNA to obtain a single line of pixels per frame; iii), subtracting background values; and iv), pasting these pixel lines into consecutive columns of a single image. Thus, in the kymograph pixel columns represent the total fluorescence intensity of the DNA, whereas rows indicate time. From the kymograph, the total DNA length incorporated in the condensate was calculated by comparing the fluorescence intensity of the bright condensate with that of the uncondensed DNA on both sides of it, averaged over a width of 7 pixels. This way, inhomogeneities of the excitation light are corrected for.

Step analysis

For each data point with force F and extension x the apparent DNA length L is calculated by rewriting the well-known interpolation formula for worm-like chain elasticity (37) into

$$L(x,F) = x\left(1-\sqrt{\frac{k_BT}{4l_pF}}\right)^{-1}\left(1+\frac{F}{K}\right),$$

with k_BT the thermal energy and K the stretch modulus of double stranded DNA (38,39). For uncondensed DNA this simply results in a constant value L_0 (~16.4 μm for λ-DNA) for all extensions. In a partially condensed λ-DNA molecule, the uncondensed fraction of the DNA still obeys the worm-like chain, but a DNA length x is lost into a small ($d \ll L$) and inextensible condensate. The measured elasticity then corresponds to that of a DNA molecule with length $L = L_0 - x$. Changes in L over time thus correspond to DNA being incorporated into or released from the DNA condensate. To extract DNA loop sizes from the contour length traces, we used a semi-automated fitting procedure (40). This algorithm has been proved successful in fitting steps in noisy data (41,42). The number of steps in each trace was optimized by thoroughly inspecting the obtained fits. The step fitting algorithm sometimes had problems registering transient back steps, occasionally leading to a misfit. To test whether this has an effect on the step size distribution, we also tracked step sizes of the same traces by a different method. This was done by computing the differences between averages of the data in each (observed) plateau. In both procedures, analysis was carried out on data resampled to 128 Hz. The distribution obtained from this plateau fitting method is virtually identical to the one acquired by using the step fitting algorithm. The only significant difference is the amount of detected back steps.

RESULTS AND DISCUSSION

Condensation of fluorescently labeled DNA

We visualized the reversible spermine-induced condensation of single DNA molecules into toroidal structures with high spatial and temporal resolution using a combination of optical tweezers and epifluorescence detection (29,32). This is achieved by attaching the endpoints of single λ-DNA molecules, sparsely labeled with the fluorescent dye YOYO-1, between two streptavidin-coated beads in a multichannel flow chamber (32) (see Materials and Methods). In the presence of spermine (0.1–1 mM), the condensation force (17) keeps the sparsely stained DNA stretched and therefore visible at all end-to-end lengths. DNA condensates are expected to appear brighter, because of the increased local DNA density and thus dye concentration. Indeed, on moving the endpoints of the DNA closer together, a single bright fluorescent DNA condensate emerges (Fig. 1 and Movie S1 in the Supporting Material), a process that is fully reversible. The most immediate result of this experiment is that it provides direct evidence that DNA in solution under tension condenses into one single collapsed structure. Furthermore, the results show that in this case the surfaces of the polystyrene beads do not act as nucleation point for DNA condensation, nor do they seem to affect the process of DNA condensation in any other way. Comparison with the contour length reduction of the uncondensed part of the DNA molecule (*gray dotted line*) shows that most of the missing DNA length is indeed included in the condensate (Fig. 1 *c*, *black trace*). Condensation of fluorescently labeled DNA by protamines and spermidine has been previously reported (25,43). In these experiments condensation commences always from the end of a flow-stretched DNA molecule held by a single optical trap, a consequence of the nonuniform tension distribution in such a configuration. In our double trap setup DNA tension is evenly distributed and controlled within less than a pN, allowing condensation to occur everywhere along the DNA with equal probability. Moreover, holding from the molecule at both ends reduces the fluctuations in the DNA, permitting localization of the condensate with high accuracy.

To analyze how the condensate incorporates DNA we quantified the fractional velocity of the condensate with respect to the translocating bead. Its displacement over time was determined with subpixel resolution by fitting the spot in each image with a 2-D Gaussian. The fractional velocity of the condensate in these traces was found to be

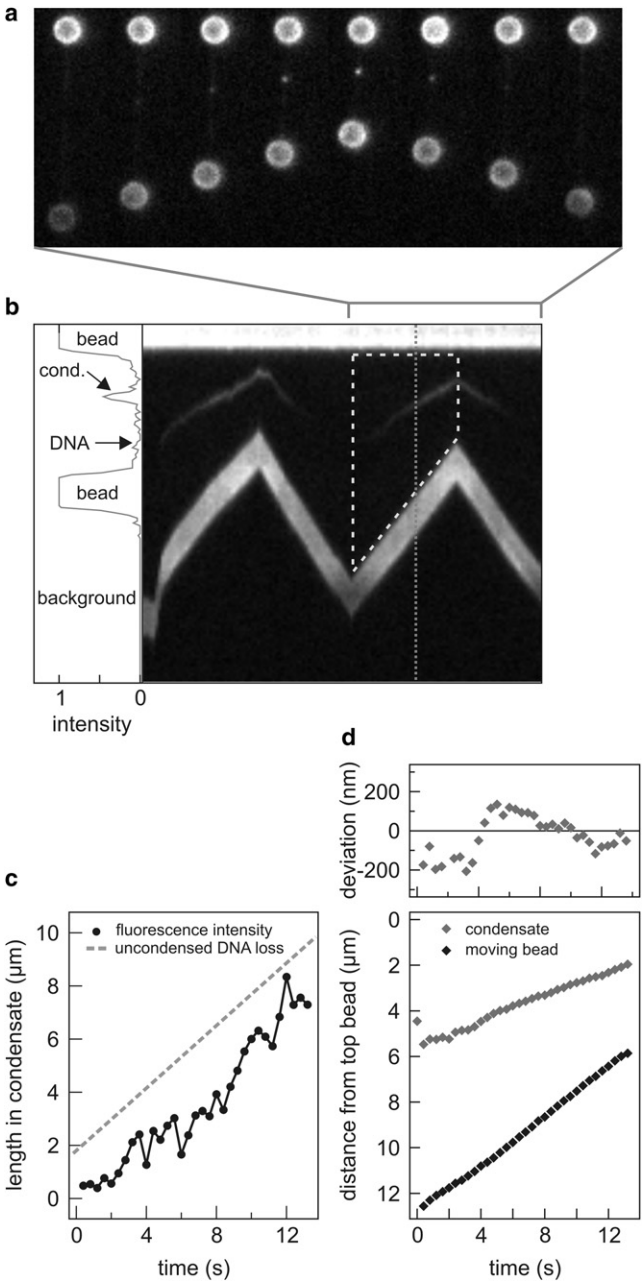

FIGURE 1 Real-time DNA condensation observed with fluorescence. (*a*) Snapshots from a movie showing condensation in a single λ-DNA molecule fixed between two beads (Movie S1). As the extension is reduced by moving the lower bead, a bright condensate appears along the DNA contour, which increases in intensity. On DNA stretching at approximately the same rate, the intensity of the spot fades again, until only uncondensed DNA is left. Note that at all times the uncondensed DNA remains in focus. The constant condensation force (45,51) suppresses lateral fluctuations of the DNA that occur in buffer without condensing agent. (*b*) Kymograph of the complete movie, (duration = 20 s), showing repeated condensation and decondensation of the same DNA molecule. The fraction of the movie in the top panel is indicated. The inset on the left shows the intensity along the dotted line. The slope of the condensate is half that of the moving bead, implying that DNA condenses from both sides of the condensate at equal rates. Similar results were obtained from other traces where the condensate was not situated in the middle of the DNA contour ($n = 7$). The dashed line shows the section that is used for the analysis in *c* and *d*. (*c*) Quantitative analysis of the fluorescence intensity per pixel calibrated to the amount of DNA per pixel during condensation. Dashed gray line: DNA length in the condensate calculated from loss of uncondensed DNA length. Black data points: total fluorescence intensity of the DNA condensate in units of length, calculated from the kymograph (see Materials and Methods for details). Quenching of dyes in the condensate due to close packing in the condensate might cause the observed fluorescence to be slightly less than expected. (*d*) Bottom: extracted positions of the moving bead and the DNA condensate of the dashed section indicated in *b*. Top: condensate displacement with respect to the expected position for equal left and right condensation rates (fractional velocity = 0.5). Slight deviations from the zero line indicate that occasionally the condensate might briefly favor one direction, but generally shows no preference.

0.50 ± 0.02, indicating that there is no preference from which of the two ends the DNA is added, i.e., the condensate reels in DNA from both sides, showing only small temporary directional fluctuations in the range of the localization accuracy of the condensate (Fig. 1 *d*). The same holds for decondensation: DNA condensates unravel from both ends at equal rates.

The kinetics of DNA condensation formation in relaxed DNA molecules can be probed by changing buffer conditions for a single DNA molecule held in optical tweezers. When a relaxed DNA molecule is rapidly moved into a buffer containing 100 μM spermine (<1 s) using our laminar flow chamber, we observed the immediate formation of a DNA condensate. Likewise, on removal of the condensed molecule from the spermine solution the condensate disappears just as quickly, and the worm-like chain (WLC) behavior of the DNA is restored. Using light-scattering techniques, condensation rates faster than 1 min^{-1}, the maximal attainable resolution, have been reported. Our results indicate that association and dissociation kinetics of condensing agent, in low ionic strength buffer, can be two orders of magnitude faster (6,44). Similar condensation behavior has been observed for DNA condensation by protamines (43).

Force-extension analysis

Using fluorescence, we directly visualized the formation of DNA-condensates, but the initial formation and perhaps the structure of such a condensate can be studied by analyzing force-extension curves with high spatial resolution. To this end we let the DNA condense by reducing the end-to-end distance in a controlled fashion using two high-stiffness traps (~300 pN/μm). The force-extension curve of λ-DNA in the presence of 1 mM spermine (Fig. 2) shows a marked hysteresis. Relaxation of an uncondensed DNA molecule below a certain extension triggers an abrupt force increase (<0.1 s) up to a rugged force plateau at ~4 pN, similar to forces reported for other condensing agents (17,18,22). We attribute this event to the sudden initiation of a spermine-induced DNA condensate, as also observed in the fluorescence data. At the force plateau, the condensation force is balanced by the external DNA tension exerted by the optical traps. Markedly, on stretching of the condensed molecule, the force

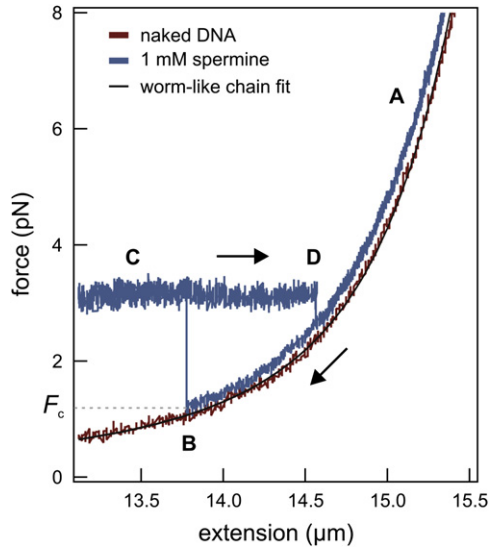

FIGURE 2 Toroid kinetics. High-resolution force-extension curves of λ-DNA with (*blue*) and without (*red*) 1 mM spermine in the solution. The extension of fully stretched DNA is slowly decreased until the tension reaches a critical force F_c at ~85% of the contour length (here 13.8 μm). At this point, the WLC behavior (*A*) suddenly disappears and the force rises abruptly (within 50–100 ms) to a value of ~3.1 pN (*B*). This marked force jump indicates the collapse of part of the DNA into a condensate. With any further reduction in the extension, the force on the DNA stays roughly constant at forces of generally 3–5 pN (*C*). When the DNA is stretched again, this force balance remains stable up to significantly higher extensions (~90% of the contour length, here 14.6 μm), until a distinct force reduction down onto the WLC curve signifies the disruption of the last piece of condensed DNA (*D*).

plateau remains present at extensions considerably larger than the end-to-end length at nucleation. Finally, a distinct force drop signifies the complete disruption of the condensate.

The force-extension hysteresis, which is reproducibly observed in all stretch-release cycles (see Fig. 3 *a*), can be explained as follows: a gradual decrease in end-to-end distance results in increasing slack in the DNA molecule, modulating the energy landscape until at a critical force F_c the energy barrier to an unfavorable transition state has been lowered enough to initiate condensation. The formation of the DNA condensate under tension is thus nucleation-limited. This conclusion is further supported by the results of the same experiment carried out under constant force conditions (see Fig. S1 and Movie S2). In this case, a larger fraction of the DNA abruptly (<0.5 s) condenses when the imposed force drops below the critical force F_c (distribution shown in Fig. S2). Our results are consistent with condensation behavior found in earlier constant-force experiments with various condensing agents (19,25,43,45), and are in good agreement with the finding that the onset of DNA condensation is the formation of a DNA loop due to random fluctuations of the polymer (45).

We also used force-extension analysis to study the condensation process after nucleation. We found that the observed ruggedness of the force plateau (18) in fact consists of series of sawtooth-like steps. To elucidate this feature, the force-extension data were converted into effective contour length (see Materials and Methods). Contour length traces of the relaxation of DNA in the presence of 1 mM spermine (Fig. 4 *a*) show clearly that the DNA molecule condenses in a stepwise manner: individual DNA segments of a defined length are added to the growing condensate one at a time. The stepwise behavior can be fitted with a step-fitting algorithm (40), yielding a broad distribution of step sizes (Fig. 4 *b*) with a dominant peak at ~40 nm and a substantial number of back steps of the same length.

If the peak in the distribution of step sizes represents loops added onto the condensate, the step size would correspond to loops with a diameter of only 12 nm. How does this small step size fit with the observed larger toroids (50–100 nm in diameter) reported for bulk experiments (28,46)? Compared to bulk studies where the DNA is free in solution during condensation, the minimum energy state for condensed DNA is markedly altered for DNA kept under tension. Whereas bending of relaxed DNA disfavors the formation of very small DNA loops, under tension the reduction of the end-to-end distance due to looping requires work that

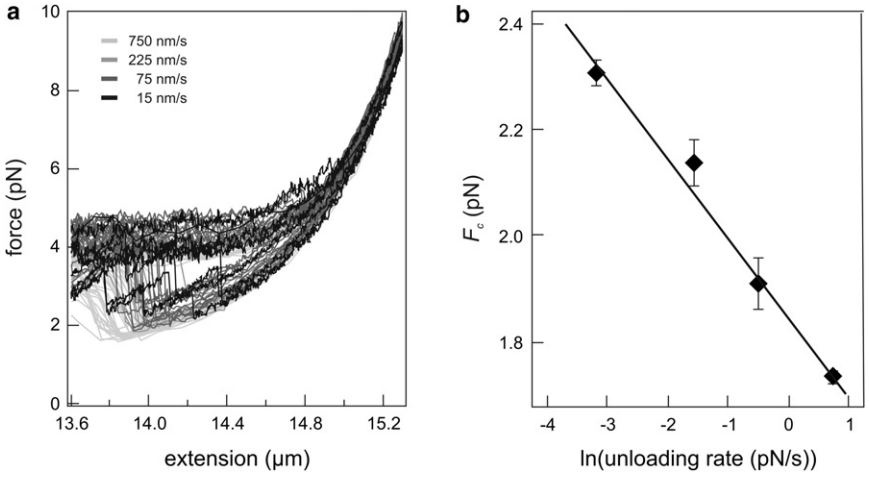

FIGURE 3 DNA relaxation speed dependence of nucleation hysteresis. (*a*) The graph shows force-extension data from repeated stretch-release cycles with different speeds on the same λ-DNA molecule. In this dynamic force spectroscopy approach, the critical condensation force F_c depends on the relaxation speed of the DNA. (*b*) Dynamic force spectroscopy on condensing DNA. The kinetic barrier in the energy landscape impeding DNA condensation is lowered by reducing the force. By fitting the slope of F_c versus the natural logarithm of the unloading rate with a line (linear correlation coefficient $r = -0.93$, normalized $\chi^2 = 0.9$), the distance to this barrier is found to be ~27 nm.

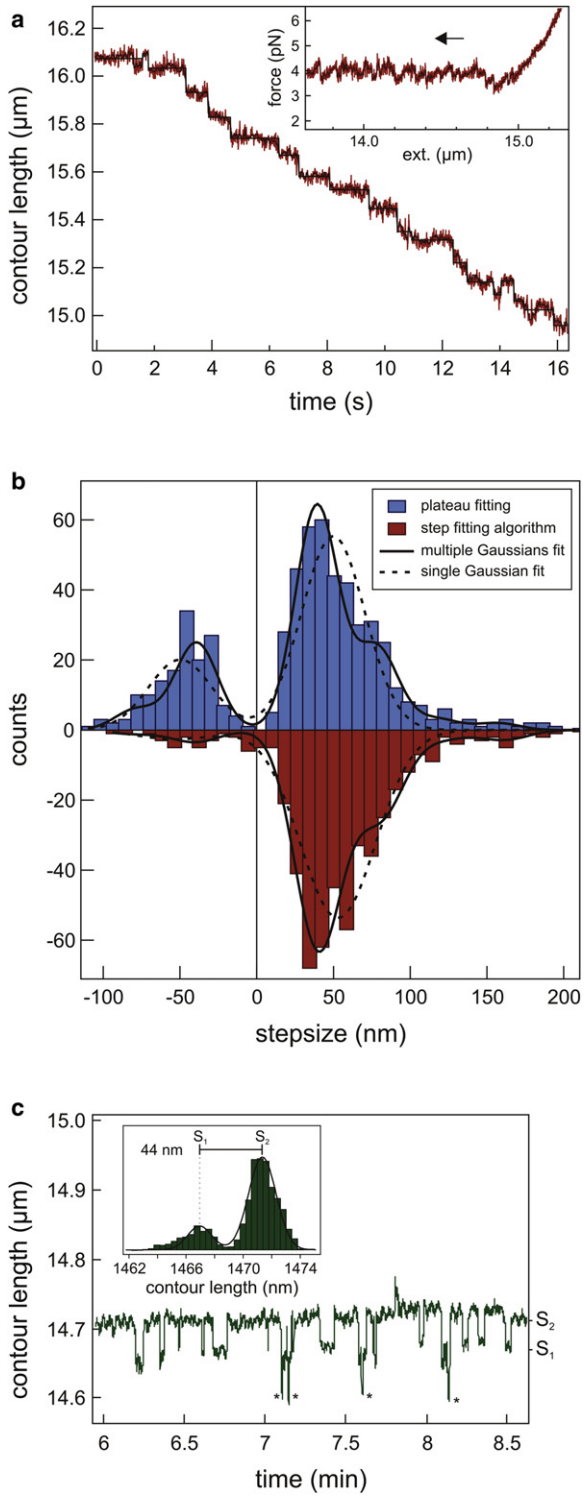

FIGURE 4 Stepwise DNA condensation. (*a*) Contour length plot of condensing DNA, constructed from the measured force and extension data. Data is shown at 128 Hz (*red*), and averaged to 16 Hz, rank 2 median filtered (*dark-red*). The data show that DNA condensation proceeds in discrete steps. The solid black line is the output of the step fitting algorithm. Transient back steps are not handled well (see *top left* and *bottom right* of the trace). The fits are therefore checked manually using a plateau fitting method (p.f.m.).The inset shows the corresponding force-extension curve. (*b*) Histograms of step sizes, acquired from several condensation traces on different DNA molecules (~10 traces, multiple micrometers per trace). The distributions obtained from plateau fitting method (top, 592 steps) and step fitting algorithm (*bottom*, 501 steps) virtually overlap, but the plateau fitting method yields a higher amount of back-steps. The data is well fit by a function consisting of multiple Gaussians having equal widths σ, spaced at integer multiples of the elementary step size x_0 (*solid curves*). Obtained parameters are: $x_0 = 40 \pm 1$ nm, $\sigma = 22$ nm with normalized $\chi^2 = 1.1$ (step fitting algorithm) and $x_0 = 39 \pm 1$ nm, $\sigma = 20$ nm with normalized $\chi^2 = 1.3$ (plateau fitting method). Fitting with only a single positive and negative Gaussian (*dashed curves*) yields a substantially worse fit (normalized $\chi^2 = 2.0$ and 2.4, respectively), indicating that the shoulder at 80 nm is significant. (*c*) Reversible wrapping of a single DNA loop. The effective contour length of the DNA switches between two distinct values. The distance between the two peaks in the dwell time histogram (*inset*) is 44 nm, indicative of a single toroid loop. Occasionally, a second loop is transiently added to the toroid (marked with *stars*).

has to be carried out against the opposing external force. These two energy contributions (bending and extension reduction) determine the energetically most favorable loop size. The total energy of a circular DNA loop with diameter d and persistence length l_p under an applied force F is

$$E_{\text{loop}} = \frac{2\pi k_b T l_p}{d} + \pi F d. \quad (1)$$

Energy minimization leads to the most probable diameter of a loop (45):

$$d = 2\sqrt{\frac{k_b T l_p}{2F}}. \quad (2)$$

For an external force of 2–5 pN as applied here and $l_p \approx 50$ nm, Eq. 2 results in $d = 14$–9 nm, or a circumference of 30–45 nm, almost an order of magnitude smaller than the diameter of DNA toroids in the absence of tension (8,28). The optimal loop length for DNA under an applied tension matches very well with a condensation scheme in which condensation proceeds by wrapping equally sized small DNA loops of ~40 nm onto a toroidal condensate. When plotting the time evolution of steps, we observe that this is indeed the case; the size of the loops added to the condensate remains constant (Fig. 5). This result is consistent with the earlier finding that a small nucleation loop leads to small toroids (47).

We can use this result to explain the broad distribution of step sizes to arise from the winding of single and multiple loops of the same diameter. Based on this interpretation the distribution should be well described by multiple equidistant Gaussians with equal widths. Indeed we find a DNA loop length of 40 ± 1 nm (SE) (see Fig. 4 *a*), as predicted above. An identical stepwise increase of the contour length (39 ± 1 nm) is observed when the condensed DNA is disrupted (see Fig. S3).

Model for toroids under tension

We can understand some of the features observed in our experiments in terms of a simple model for toroids under

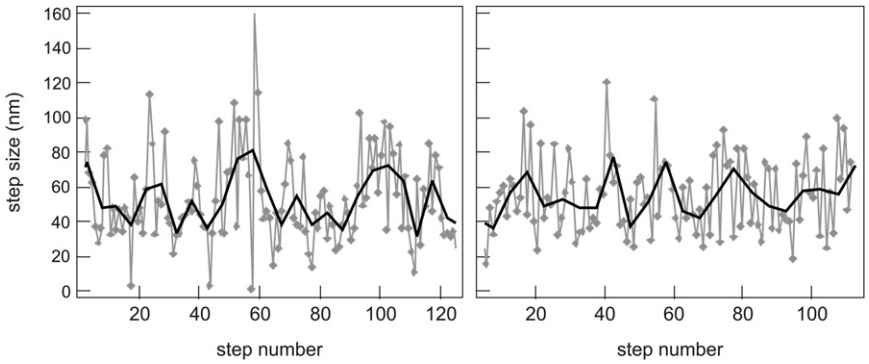

FIGURE 5 Time evolution of observed steps in a single condensing DNA molecule. Data points show consecutive positive step sizes obtained from two different traces, acquired with the step fitting algorithm. Black lines indicate the mean step size, averaged over five steps. This graph indicates that there is no significant trend in the size of individual loops wrapped onto a DNA toroid.

tension, in which we incorporate the bending energy for torus formation and the assumed attractive interaction between DNA segments in the presence of condensing agent. This is based on a previous model by Schnurr et al. (48) for condensed states in the absence of tension, to which we have also included the mechanical work against the tension due to the condensation of DNA into a toroid. More details on the model can be found in Battle et al. (49). Specifically, for a given total DNA length L_T in the toroid, the bending energy is given by $2\kappa\pi^2N^2/L_T$, where $\kappa = l_p k_B T$ is the bending stiffness and N is the number of (complete) loops in the torus. The interaction is modeled by a binding energy $-\gamma$ per unit length of an adjacent pair of DNA strands in the condensate. The number of these bonds between adjacent segments depends on the geometry of the cross section of the toroid, as illustrated in Fig. 6, where a symmetric $N = 7$ structure with 12 such bonds is shown. Using this model, we calculate the optimal toroid states for given values of L_T and tension F applied to the free ends.

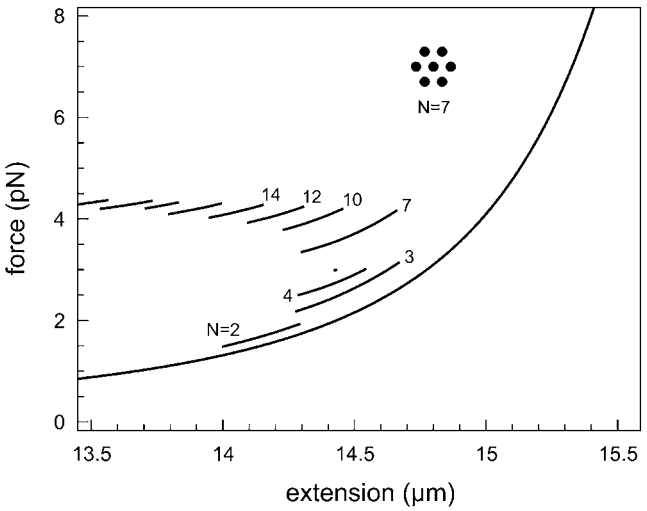

FIGURE 6 Predicted force-extension curves for the most stable toroid states, which have been labeled by the first few corresponding winding numbers N. Here, we have assumed that the DNA toroid(s) comprising length L_T are in series with freely fluctuating uncondensed DNA of length $L - L_T$, with the total DNA contour length L equal to 16.22 μm and l_p = 40 nm (consistent with values found earlier in similar conditions (52)), and $\gamma = 1.65$ pN (49). Also included is a sketch of a highly symmetric cross section of a torus with $N = 7$.

In this model, it is useful to define a characteristic energy scale $U_c = \sqrt{\kappa\gamma}$, which we call the condensation energy, as well as a characteristic length scale $L_c = \sqrt{\kappa/\gamma}$, the condensation length (48). We then measure lengths in units of L_c and forces or tension in units of $U_c/L_c = \gamma$. Starting with a large N toroid, as the tension F increases to a critical value close to 3γ (49), we find that the toroid becomes unstable and begins to unravel. In this process, however, we find a cascade of discrete, metastable toroid states, very similar to the experimental observations as illustrated in Fig. 4. The results of the model are shown in Fig. 6 where we plot the expected force-extension curves for the most stable toroid states within the model.

There is only a single unknown parameter in the model, the interaction energy γ. Because this parameter completely determines the predicted force plateau, we adjust this to account for the observed $\cong$ 4.5 pN plateau. In the figure, a few specific values of the winding number N are shown. Our model predicts discrete transitions between optimal torus states by $\Delta N = 1$. However, many of the intermediate states (e.g., between $N = 7$ and 10) are predicted to be highly unstable and will make rapid transitions to lower values of N during unraveling. This is consistent with the observed step size distribution of toroid disruption (Fig. 4 *b*), where often we find steps of 80 nm ($\Delta N = 2$). Furthermore, the prediction of multiple metastable states predicted near full unraveling of the toroid is consistent with the appearance of hysteresis (e.g., in Fig. 2). Vice versa, Fig. 6 also explains the large condensation nucleation step size (average ~400 nm; see Fig. S2) when relaxing the DNA molecule in condensing conditions. On reaching $N = 2$, many toroid loops are rapidly formed, bypassing the other states and finally terminating around $N = 10$.

Visualizing metastable toroid states

In many of the DNA relaxation and stretching (toroid formation and disruption) traces, transient back steps are observed (e.g., Fig. 4 *a*). The contour length change in these steps is found to be comparable to that of a single toroid loop, ~40 nm (Fig. 4 *b* and Fig. S3 *b*). This apparent reversible

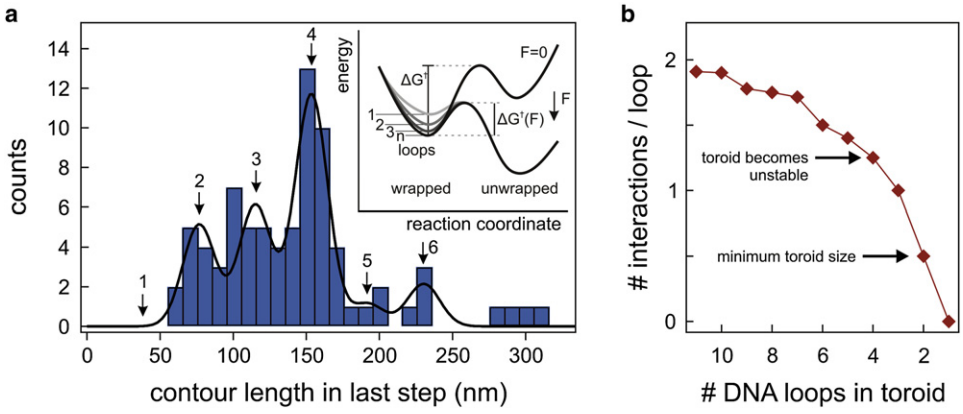

FIGURE 7 Minimum stable toroid size. (*a*) Distribution of observed last-step sizes in the toroid disruption process ($N = 74$). No steps of 40 nm are detected (indicated with the arrow at 1) here (compare with Fig. 4 *b* and Fig. S3). The most common last step is ~150 nm, comprising four DNA loops. The data is fit with multiple Gaussians, resulting in a step size $x_0 = 38 \pm 1$ nm with width $\sigma = 17$ nm. Inset: Schematic diagram of the energy landscape during the unraveling of a loop. Extending the DNA increases the force on the toroidal condensate, resulting in a lowered energy barrier to the unwrapped state. (*b*) Computed number of interactions per remaining DNA loop in a toroid-shaped condensate, assuming a hexagonally packed structure. The curve shows a steep decline starting roughly at four loops.

wrapping of DNA loops onto the toroid can most clearly be demonstrated when the DNA end-to-end distance is held fixed when a condensate is present, i.e., somewhere in the force plateau (Fig. 4 *c*). The contour length is observed to toggle between two distinct values, in this case 44 nm apart, signifying the reversible addition and removal of a single toroid loop. As the winding is carried out against an external force of ~5 pN, the energy of such a loop, calculated as $F \times (S_2 - S_1)$, is enormous: ~60 k_BT, or 0.4 k_BT/bp (a few times higher than determined for condensation by spermidine^{3+} (18)). However, the inclusion of a DNA loop into the toroid causes a shortening of the uncondensed DNA, which increases the mechanical strain in the molecule. Due to this effect the difference between the two energy states (S_1 and S_2) becomes small enough to be overcome by thermal fluctuations. From the relative occupancies of the two states in the trace (Fig. 4 *c*, *inset*) we calculate the energy difference between S_1 and S_2 to be only ~1.5 k_BT in this case.

To investigate the energy landscape of toroid formation, we carried out dynamic force spectroscopy (50) on the formation of the initial toroid. As DNA tension influences transitions from one state to another, the critical force F_c (see Fig. 2), should depend on the rate at which this force is reduced. We measured F_c as a function of this unloading rate in several stretch-release cycles on the same λ-DNA molecule (Fig. 3 *a*). The resulting spectrum reveals that the nucleation hysteresis indeed depends on the unloading rate (Fig. 3 *b*). It can be characterized by a linear fit, indicating that there is a single kinetic barrier in the energy landscape of the transition state. From the slope of the fit we determine the distance to the transition state to be 27 ± 3 nm, about two-thirds of the observed toroid loop length. We hypothesize that, when thermal fluctuations are able to create a local molecular slack >~27 nm, a first DNA loop can be formed. In the presence of spermine, the attraction between close DNA segments somewhat stabilizes this loop, facilitating expansion of the overlapping DNA regions. The condensate then quickly recruits more of its neighboring DNA until a force balance between condensate and traps is achieved. Apparently, this process starts as soon as a single loop is present.

The end of the force plateau

To further investigate the nature of DNA condensates we focus on an intriguing feature of the force-extension curve: the point where, when stretching the polymer, the force plateau disappears and WLC-elasticity re-emerges (Fig. 2 *a*, *step D*). The sudden transition, marked by an irreversible drop in tension, suggests that this last step in the disruption process represents the destruction of the smallest stable condensed structure at that force. Fig. 7 *a* displays a distribution of the contour length gained in such last steps. The measured distribution fits the same function of multiple Gaussians as before; again the data are consistent with an elementary step size of ~40 nm. Interestingly, no steps <50 nm are observed; the first peak is located at 76 nm. This implies that a stable toroid structure comprises a minimum of two DNA loops. Moreover, larger steps ($\Delta N > 2$) are frequently observed. This behavior can be understood when a hexagonally packed toroidal condensate structure is assumed. Because of removal of shared nearest-neighbor interactions, the average binding energy per remaining DNA loop decreases nonlinearly with the number of turns still present in the toroid (8,28,46). The number of interstrand interactions per DNA loop in such a structure declines steeply when only approximately four DNA loops are left (Fig. 7 *b*). Eventually, the energy barrier for removing the next DNA loop in the disruption process becomes sufficiently small for thermal fluctuations to release all of the residual loops

rapidly after each other (Fig. 7 *a*, *inset*). The experimental results are in agreement with this scheme; the most frequent step size we find is equal to 150 nm ($\Delta N \cong 4$). Interestingly, our toroid model, represented in Fig. 6, qualitatively predicts this behavior: as the lower N states are disrupted, some states (e.g., $N = 5$ and $N = 6$, but also $N = 1$) will be bypassed. Consistent with the model we rarely observe $N = 5$ or $N = 6$, and never $N = 1$ loops as last disruption step.

Implications for toroids under tension

The disruption of DNA condensates with optical tweezers has been reported earlier (17,18) and circumferences of individual turns of DNA toroids in low monovalent salt buffer were found to peak ~300 nm. What is the explanation for the large mismatch with the much smaller step sizes that we find (suggesting much smaller DNA toroids)? From the previous studies it was thought that there are two regimes in DNA condensation. The first, so-called stick-release events, observed in high concentrations of condensing agent, were viewed on as the discrete unfolding of the condensate. The second regime, the constant force plateau observed at lower concentrations, was associated with a continuous transition between condensed and relaxed DNA. We show that there is no qualitative difference between plateau and stick-slip. Both regimes can be explained by characteristic stepwise unraveling of condensed DNA. At high concentrations of condensing agent, a stronger attraction between DNA tracts in the toroid may cause disruption to occur in larger steps comprising multiple toroid loops, resulting on average in larger unfolding steps. This conclusion is further supported by analysis of our force-extension curves at elevated (>1 mM) concentrations of condensing agent in which we sometimes observed modest stick-slip behavior. By evaluating those events, we could qualitatively reproduce the shape of the step size distribution obtained previously (18) with in this case a most frequent step size of 150–200 nm (see Fig. S4).

CONCLUSIONS

We have visualized DNA condensation in real-time and have determined that DNA is reeled in from both ends at the same time. Using high resolution, quantitative force measurements of the stepwise condensation process, we have shown that a toroidal structure is likely to be formed in condensing DNA kept under tension. Moreover, by relating our results to a simple toroid model we have qualitatively explained the shape of the force-extension curve of a condensed DNA molecule. The toroid forming mechanism could also be aiding DNA condensation in sperm cells, where the chromosomal DNA is compacted into numerous toroids spaced closely together (12). Furthermore, DNA toroids are a major candidate as a delivery vehicle in gene therapy (26–28). Extensive and quantitative assays of formation and deformation kinetics will be relevant for developments in this direction.

SUPPORTING MATERIAL

Four figures and two movies are available at http://www.biophysj.org/biophysj/supplemental/S0006-3495(10)00148-7.

We thank H. Schiessel, K. Besteman, and S. G. Lemay for useful discussions.

This work was supported by the Nederlandse Organisatie voor Wetenschappelijk Onderzoek Vernieuwingsimpuls and VICI grants. This work is part of the research program of the Stichting voor Fundamenteel Onderzoek der Materie.

REFERENCES

1. Hougaard, D. M. 1992. Polyamine cytochemistry: localization and possible functions of polyamines. *Int. Rev. Cytol.* 138:51–88.
2. Thomas, T., and T. J. Thomas. 2001. Polyamines in cell growth and cell death: molecular mechanisms and therapeutic applications. *Cell. Mol. Life Sci.* 58:244–258.
3. Wilson, R. W., and V. A. Bloomfield. 1979. Counterion-induced condensation of deoxyribonucleic acid. a light-scattering study. *Biochemistry.* 18:2192–2196.
4. Chattoraj, D. K., L. C. Gosule, and A. Schellman. 1978. DNA condensation with polyamines. II. Electron microscopic studies. *J. Mol. Biol.* 121:327–337.
5. Gosule, L. C., and J. A. Schellman. 1976. Compact form of DNA induced by spermidine. *Nature*. 259:333–335.
6. Widom, J., and R. L. Baldwin. 1980. Cation-induced toroidal condensation of DNA studies with $Co^{3+}(NH_3)^6$. *J. Mol. Biol.* 144:431–453.
7. Bottcher, C., C. Endisch, …, M. Eaton. 1998. High-yield preparation of oligomeric C-type DNA toroids and their characterization by cryoelectron microscopy. *J. Am. Chem. Soc.* 120:12–17.
8. Hud, N. V., and K. H. Downing. 2001. Cryoelectron microscopy of lambda phage DNA condensates in vitreous ice: the fine structure of DNA toroids. *Proc. Natl. Acad. Sci. USA.* 98:14925–14930.
9. Marx, K. A., and G. C. Ruben. 1983. Evidence for hydrated spermidine-calf thymus DNA toruses organized by circumferential DNA wrapping. *Nucleic Acids Res.* 11:1839–1854.
10. Marx, K. A., and G. C. Ruben. 1984. Studies of DNA organization in hydrated spermidine-condensed DNA toruses and spermidine-DNA fibers. *J. Biomol. Struct. Dyn.* 1:1109–1132.
11. Schellman, J. A., and N. Parthasarathy. 1984. X-ray diffraction studies on cation-collapsed DNA. *J. Mol. Biol.* 175:313–329.
12. Hud, N. V., M. J. Allen, …, R. Balhorn. 1993. Identification of the elemental packing unit of DNA in mammalian sperm cells by atomic force microscopy. *Biochem. Biophys. Res. Commun.* 193: 1347–1354.
13. Allison, S. A., J. C. Herr, and J. M. Schurr. 1981. Structure of viral phi 29 DNA condensed by simple triamines: a light-scattering and electron-microscopy study. *Biopolymers*. 20:469–488.
14. Arscott, P. G., A. Z. Li, and V. A. Bloomfield. 1990. Condensation of DNA by trivalent cations. 1. Effects of DNA length and topology on the size and shape of condensed particles. *Biopolymers*. 30:619–630.
15. Post, C. B., and B. H. Zimm. 1982. Light-scattering study of DNA condensation: competition between collapse and aggregation. *Biopolymers*. 21:2139–2160.
16. Widom, J., and R. L. Baldwin. 1983. Monomolecular condensation of lambda-DNA induced by cobalt hexamine. *Biopolymers.* 22: 1595–1620.
17. Baumann, C. G., V. A. Bloomfield, …, S. M. Block. 2000. Stretching of single collapsed DNA molecules. *Biophys. J.* 78:1965–1978.

18. Murayama, Y., Y. Sakamaki, and M. Sano. 2003. Elastic response of single DNA molecules exhibits a reentrant collapsing transition. *Phys. Rev. Lett.* 90:018102.

19. Husale, S., W. Grange, …, M. Hegner. 2008. Interaction of cationic surfactants with DNA: a single-molecule study. *Nucleic Acids Res.* 36:1443–1449.

20. Bloomfield, V. A. 1997. DNA condensation by multivalent cations. *Biopolymers.* 44:269–282.

21. Plum, G. E., P. G. Arscott, and V. A. Bloomfield. 1990. Condensation of DNA by trivalent cations. 2. Effects of cation structure. *Biopolymers.* 30:631–643.

22. Baumann, C. G., S. B. Smith, …, C. Bustamante. 1997. Ionic effects on the elasticity of single DNA molecules. *Proc. Natl. Acad. Sci. USA.* 94:6185–6190.

23. Fu, W. B., X. L. Wang, …, M. Li. 2006. Compaction dynamics of single DNA molecules under tension. *J. Am. Chem. Soc.* 128:15040–15041.

24. Ritort, F., S. Mihardja, …, C. Bustamante. 2006. Condensation transition in DNA-polyaminoamide dendrimer fibers studied using optical tweezers. *Phys. Rev. Lett.* 96:118301.

25. Su, T. J., E. Theofanidou, …, J. Crain. 2004. Single molecule fluorescence imaging and its application to the study of DNA condensation. *J. Fluoresc.* 14:65–69.

26. Mahato, R. I., Y. Takakura, and M. Hashida. 1997. Nonviral vectors for in vivo gene delivery: physicochemical and pharmacokinetic considerations. *Crit. Rev. Ther. Drug Carrier Syst.* 14:133–172.

27. Vijayanathan, V., T. Thomas, and T. J. Thomas. 2002. DNA nanoparticles and development of DNA delivery vehicles for gene therapy. *Biochemistry.* 41:14085–14094.

28. Hud, N. V., and I. D. Vilfan. 2005. Toroidal DNA condensates: unraveling the fine structure and the role of nucleation in determining size. *Annu. Rev. Biophys. Biomol. Struct.* 34:295–318.

29. Mameren, J., M. Modesti, …, E. J. Peterman. 2006. Dissecting elastic heterogeneity along DNA molecules coated partly with Rad51 using concurrent fluorescence microscopy and optical tweezers. *Biophys. J.* 91:L78–L80.

30. van Mameren, J., M. Modesti, …, G. J. Wuite. 2009. Counting RAD51 proteins disassembling from nucleoprotein filaments under tension. *Nature.* 457:745–748.

31. van den Broek, B., M. C. Noom, and G. J. L. Wuite. 2005. DNA-tension dependence of restriction enzyme activity reveals mechanochemical properties of the reaction pathway. *Nucleic Acids Res.* 33:2676–2684.

32. Noom, M. C., B. van den Broek, …, G. J. Wuite. 2007. Visualizing single DNA-bound proteins using DNA as a scanning probe. *Nat. Methods.* 4:1031–1036.

33. Widom, J., and R. L. Baldwin. 1983. Inhibition of cation-induced DNA condensation by intercalating dyes. *Biopolymers.* 22:1621–1632.

34. Yoshinaga, N., T. Akitaya, and K. Yoshikawa. 2001. Intercalating fluorescence dye YOYO-1 prevents the folding transition in giant duplex DNA. *Biochem. Biophys. Res. Commun.* 286:264–267.

35. Bennink, M. L., O. D. Schärer, …, J. Greve. 1999. Single-molecule manipulation of double-stranded DNA using optical tweezers: interaction studies of DNA with RecA and YOYO-1. *Cytometry.* 36:200–208.

36. Thompson, R. E., D. R. Larson, and W. W. Webb. 2002. Precise nanometer localization analysis for individual fluorescent probes. *Biophys. J.* 82:2775–2783.

37. Bustamante, C., J. F. Marko, …, S. Smith. 1994. Entropic elasticity of lambda-phage DNA. *Science.* 265:1599–1600.

38. Odijk, T. 1995. Stiff chains and filaments under tension. *Macromolecules.* 28:7016–7018.

39. Smith, S. B., Y. Cui, and C. Bustamante. 1996. Overstretching B-DNA: the elastic response of individual double-stranded and single-stranded DNA molecules. *Science.* 271:795–799.

40. Kerssemakers, J. W., E. L. Munteanu, …, M. Dogterom. 2006. Assembly dynamics of microtubules at molecular resolution. *Nature.* 442:709–712.

41. Dame, R. T., M. C. Noom, and G. J. Wuite. 2006. Bacterial chromatin organization by H-NS protein unraveled using dual DNA manipulation. *Nature.* 444:387–390.

42. Sowa, Y., A. D. Rowe, …, R. M. Berry. 2005. Direct observation of steps in rotation of the bacterial flagellar motor. *Nature.* 437:916–919.

43. Brewer, L. R., M. Corzett, and R. Balhorn. 1999. Protamine-induced condensation and decondensation of the same DNA molecule. *Science.* 286:120–123.

44. He, S., P. G. Arscott, and V. A. Bloomfield. 2000. Condensation of DNA by multivalent cations: experimental studies of condensation kinetics. *Biopolymers.* 53:329–341.

45. Besteman, K., S. Hage, …, S. G. Lemay. 2007. Role of tension and twist in single-molecule DNA condensation. *Phys. Rev. Lett.* 98:058103.

46. Bloomfield, V. A. 1991. Condensation of DNA by multivalent cations: considerations on mechanism. *Biopolymers.* 31:1471–1481.

47. Shen, M. R., K. H. Downing, …, N. V. Hud. 2000. Nucleation of DNA condensation by static loops: formation of DNA toroids with reduced dimensions. *J. Am. Chem. Soc.* 122:4833–4834.

48. Schnurr, B., F. Gittes, and F. C. MacKintosh. 2002. Metastable intermediates in the condensation of semiflexible polymers. *Phys. Rev. E Stat. Nonlin. Soft Matter Phys.* 65:061904.

49. Battle, C., B. van den Broek, …, F. C. MacKintosh. 2009. Unraveling DNA tori under tension. *Phys. Rev. E Stat. Nonlin. Soft Matter Phys.* 80:031917.

50. Evans, E. 2001. Probing the relation between force—lifetime—and chemistry in single molecular bonds. *Annu. Rev. Biophys. Biomol. Struct.* 30:105–128.

51. Todd, B. A., and D. C. Rau. 2008. Interplay of ion binding and attraction in DNA condensed by multivalent cations. *Nucleic Acids Res.* 36:501–510.

52. Wang, M. D., H. Yin, …, S. M. Block. 1997. Stretching DNA with optical tweezers. *Biophys. J.* 72:1335–1346.